Chinese Chemical Letters 34 (2023) 108018

Contents lists available at ScienceDirect

Chinese Chemical Letters

journal homepage: www.elsevier.com/locate/cclet

Carbon-supported CoS_4-C single-atom nanozyme for dramatic improvement in CO_2 electroreduction to HCOOH: A DFT study combined with hybrid solvation model

Hao Sun, Jingyao Liu*

Institute of Theoretical Chemistry, College of Chemistry, Jilin University, Changchun 130023, China

ARTICLE INFO

Article history:
Received 25 October 2022
Revised 17 November 2022
Accepted 22 November 2022
Available online 24 November 2022

Keywords:
Single-atom catalysts
Nanozymes
Electrocatalysis
CO_2 reduction
Density functional theory

ABSTRACT

Single-atom nanozymes (SANs) have attracted extensive attention due to their characteristics of both single-atom catalysts (SACs) and enzymes. Using spin-polarized density functional theory (DFT) calculations combined with the hybrid solvation model, this work designed a series of carbon-supported Group VIII transition metals TMS_4-C SANs, similar to the TMS_4 active center of formate dehydrogenase (FADH), aiming to develop highly efficient SANs for CO_2 electroreduction. DFT calculations show that compared with TMN_4-C, TMS_4-C have FADH-like feature, which can selectively reduce CO_2 to formic acid. Particularly, CoS_4-C is the most promising SAN for CO_2 reduction, with a low limiting potential of -0.07 V, which exceeds most reported catalysts. Two descriptors of TMX_4-C (X = N, S) based on intrinsic and electronic structure properties were proposed to shed light on the origin activity of candidates. The findings presented here will provide new insights into the design of novel enzyme-like catalysts for electrochemical CO_2 reduction.

Electrochemical carbon dioxide reduction reaction (eCO_2RR) provides an attractive way to convert CO_2 into valuable fuels and chemicals using renewable energy under mild and controllable conditions. On the one hand, it can realize the efficient storage of electric energy and alleviate the energy crisis. On the other hand, it can reduce the emission of CO_2 into the atmosphere and alleviate the greenhouse effect [1,2]. Therefore, eCO_2RR has broad application prospects. Despite a considerable amount of experimental and theoretical reports [3–8], there are still some critical challenges to the technological viability of eCO_2RR. In the process of eCO_2RR, high overpotential is required to activate the stable C=O bond [9]. At the same time, the competition between hydrogen evolution reaction (HER) and multiple reaction paths leads to low Faradaic efficiency and poor product selectivity [10]. Therefore, finding economical and efficient catalysts is the key to promote the development and application of electrocatalytic CO_2 reduction technology.

Natural enzymes play a vital role in living systems due to their excellent catalytic activities and selectivity. However, the high preparation cost, easy deactivation and limited reaction conditions hinder their practical application [11]. One of the improved strategies is to develop enzyme-mimic materials that can overcome the above drawbacks. In particular, single-atom nanozymes (SANs) have recently received considerable attention [12,13]. SAN is a special kind of single-atom catalysts (SACs). It is well known that SACs have the structural characteristics of high atom dispersion and ultra-high atom utilization, and they show high activity in many catalytic reactions [14,15]. In addition to these characteristics of SACs, SANs also mimic the coordination environment or geometric configuration of the enzymes and exhibit specific product selectivity for specific reactions. Moreover, the catalytic activity of SANs can be easily regulated by the microenvironment, and the required reaction conditions are relatively mild [16]. Due to the characteristics of the structure and performance, SANs have aroused increasing research interest in the electrocatalytic field [17–19]. For example, TM-N-C metal enzymes with active sites similar to peroxidase (POD), oxidase (OXD) and porphyrin have been extensively studied. Fe-N-C SAN with FeN_4 sites showed high peroxidase-like activity of 25.33 U/mg for the electroreduction of H_2O_2 [20]. SAN with nanoframe-confined FeN_5 active sites, which was designed by Huang *et al.* [21] with a similar structure to the axial ligand–coordinated heme of cytochrome P450, showed excellent catalytic activity for oxygen reduction reaction. In addition to the N-coordinated structure, the TM-S site is also the active center of many natural enzymes, such as nitrogenase, formate dehydrogenase (FADH), and CO-dehydrogenase (CODH). Wen *et al.* [22] theoretically designed a series of graphene-supported

* Corresponding author.
E-mail address: ljy121@jlu.edu.cn (J. Liu).

https://doi.org/10.1016/j.cclet.2022.108018
1001-8417/

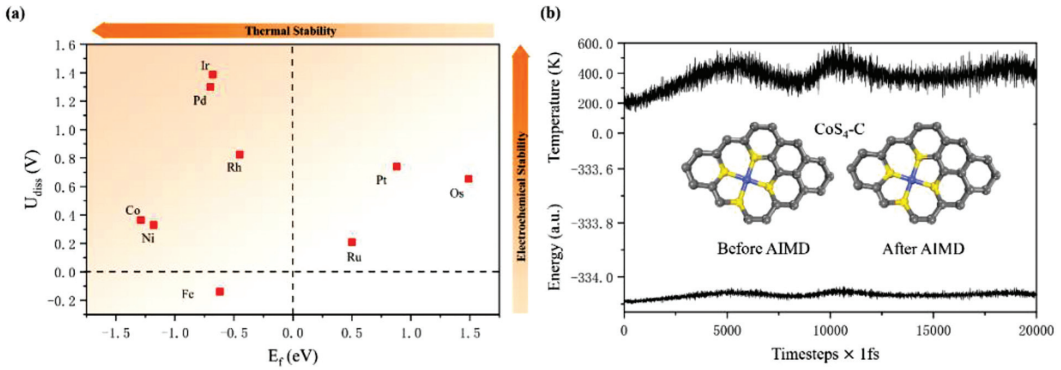

Fig. 1. (a) U_{diss} and E_f of Group VIII transition metals SANs. (b) Temperature and energy curves versus timesteps and local structures before and after AIMD for CoS_4-C.

MoX_4 (X = C, N, B, S, P) SACs, and found that MoS_4/GR with the same coordination as nitrogenase can catalyze nitrogen reduction reaction (NRR) at a low limiting potential of −0.29 V. Recently, the active sites [NiS_4] of FADH and CODH were simulated experimentally [23], and the prepared MOFs incorporated with nickel bis(dithiolene) ligands significantly improved the conversion rate and Faradaic effciency (89%) of CO_2 electroreduction to HCOOH. In addition, carbon-supported CoS_4 SAC was also successfully synthesized by pyrolysis of Co-MOF-74 in a strongly polar molten salt system [24], and the counter electrode of this SAC showed higher photo-electric conversion effciency than Pt counter electrode, and has good structural stability.

Inspired by the active site structures of FADH and CODH and the latest experimental synthesis of CoS_4, in this study, we used density functional theory (DFT) to calculate and design a series of enzyme-like single-atom catalysts supported on graphene with TMS_4-C active center for electrochemical CO_2RR, where the TM atoms are the Group VIII transition metals (TM = Co, Ni, Rh, Ir). Since eCO_2RR occurs in the electrolyte, in order to better consider the solvent effect, the hybrid solvation model was adopted in the calculation. To further clarify the influence of coordination environment on catalytic performance, we also studied the CO_2RR mechanism of typical TMN_4-C catalysts for the selected TM of above TMS_4-C SANs. DFT results show that CoS_4-C SAN has a theoretical limiting potential of −0.07 V for the highly selective electroreduction of CO_2RR to HCOOH. TMS_4-C SANs have better CO_2 catalytic performance than the corresponding TMN_4-C SACs. In addition, two descriptors of TMX_4-C (X = N, S) CO_2RR activity based on intrinsic properties were proposed. Our current results may provide new insights into the design of advanced CO_2RR electrocatalysts.

Spin-polarized density functional theory (DFT) calculations were performed by the Vienna Ab initio Simulation Package (VASP) using the generalized gradient approximation (GGA) with Perdew−Burke−Ernzerhof (PBE) functional, with a cutoff energy of 400 eV [25–28]. A Monkhorst−Pack mesh of $3 \times 3 \times 1$ *k*-points was used for geometric optimization and $9 \times 9 \times 1$ for electronic structure analysis. The long-range van der Waal's interactions were described using the DFT-D3 empirical dispersion correction [29]. The energy and force convergence criteria were set to 10^{-5} eV and 0.02 eV/Å, respectively. The vacuum was set as 20 Å to avoid interactions between periodic images in the *z* direction. Referring to the previous reports [30–32], the graphene monolayer was modeled using a $4 \times 4 \times 1$ supercell. Moreover, the hybrid solvation was adopted to describe the solvation effect. A hexagonal water bilayer containing 16 H_2O molecules was added to simulate surrounding water molecules, and Poisson–Boltzmann implicit solvation model was utilized to describe long-range interactions, as implemented in the VASPsol [33].

To evaluate the thermodynamic and electrochemical stability of SANs, we calculated the formation energy (E_f) and dissolution potential (U_{diss}, *vs.* SHE), which are defined as

$$E_f = E_{total} - E_{sub} - E_{TM} \quad (1)$$

$$U_{diss} = U^o_{diss}(\text{metal, bulk}) - E_f/eN_e \quad (2)$$

where E_{total} and E_{sub} are the energies of SAN and substrate, respectively, and E_{TM} is the energy of the single metal atom in the bulk; U^o_{diss}(metal, bulk) is the standard dissolution potential of bulk metals, and N_e is the number of electrons involved in the dissolution [34]. It can be seen that Ru-, Os- and PtS_4-C with positive E_f cannot maintain stability due to the thermodynamically favorable diffusion and aggregation of metal atoms, and FeS_4-C is easily deactivated due to the dissolution of Fe atoms under electrochemical conditions (Fig. 1a). The stability of the other 5 SANs is further confirmed through 20 ps AIMD simulations with a time step of 1 fs in the NVT ensemble at 400 K. It can be seen that Co-, Ni-, Rh- and IrS_4-C maintain stable TM-S_4 structures after 20 ps AIMD simulations (Fig. 1b and Fig. S1 in Supporting information). In addition, although PdS_4-C SAN with S-Pd-S coordination could hold stability through the AIMD simulation, it undergoes a great distortion when the intermediates are adsorbed on the surface (Fig. S2 in Supporting information). Thus, it was not considered in the following mechanism study.

Due to the single-atom characteristic of SANs, only C_1 products were considered in the current work. As shown in Scheme S1 (Supporting information), proton-electron pairs attack CO_2 to form different initial configurations (*COOH and *HCOO), resulting in different pathways of eCO_2RR, and finally generate C_1 products, HCOOH, CO, CH_3OH and CH_4 *via* multi-step proton coupled electron transfer (PCET). Fig. 2 (left) shows the free energy diagrams of CO_2RR on TMS_4-C. Reduction of intermediates (such as * H_2COO, * COH) that are too high in the free energy diagrams was not considered further. To facilitate comparison, the corresponding CO_2RR free energy curves of TMN_4-C catalyst are shown in Fig. 2 (right). The free energy change of each elementary step was calculated according to the computational hydrogen electrode (CHE) model proposed by Nørskov *et al.* [35]. The limiting potential of CO_2RR is defined as $U_L = -\Delta G_{PDS}/e$, where the ΔG_{PDS} is the free energy change of the potential-determined step (PDS).

As shown in Fig. 2a, the formation of intermediates *HCOO and *COOH on CoS_4-C SAN requires the free energy of 0.07 and 0.37 eV, respectively. The hydrogenation of these two intermediates directly forms HCOOH(dl) at the catalysts-electrolyte interface instead of adsorbed *HCOOH, which prevents the continuous hydrogenation of *HCOOH. In addition, *COOH can be further converted into *CO. However, the release of CO or further hydrogena-

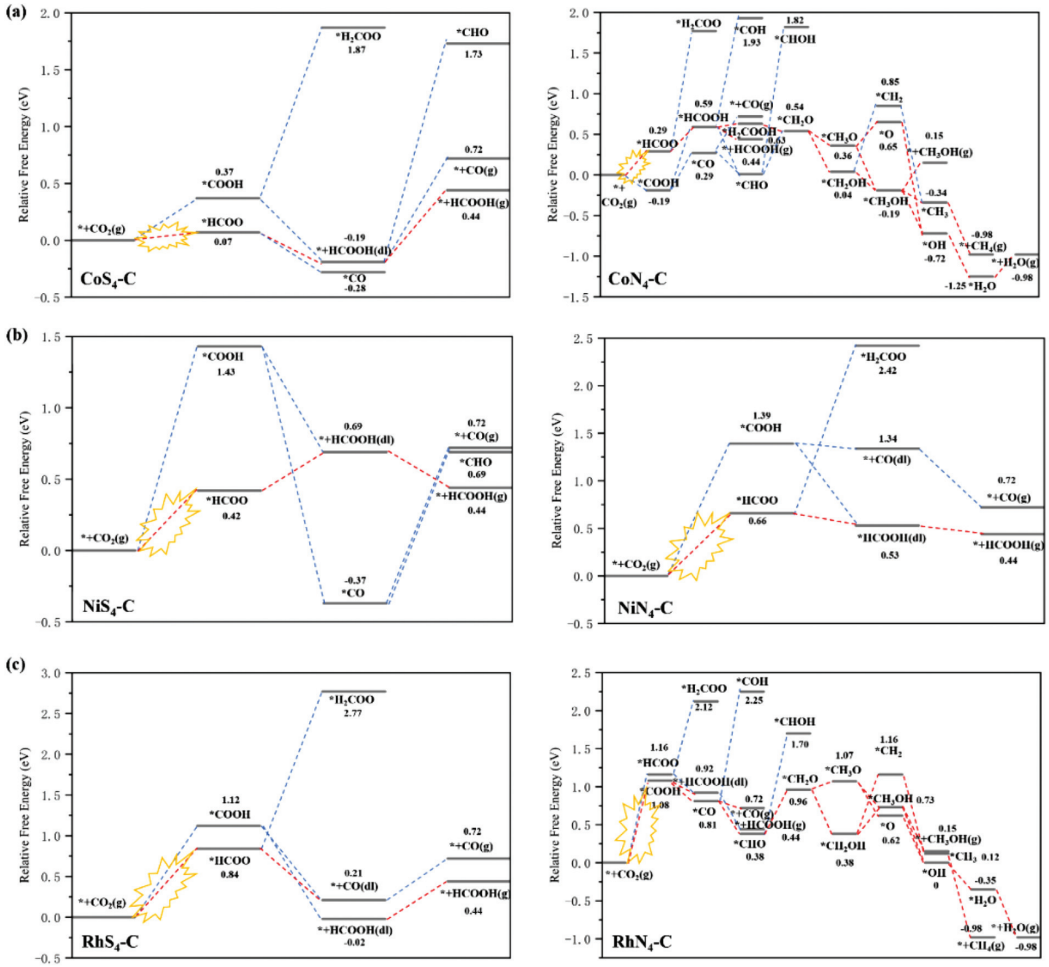

Fig. 2. Free energy diagrams of CO_2RR on (a) CoS_4-C (left) and CoN_4-C (right). (b) NiS_4-C (left) and NiN_4-C (right). (c) RhS_4-C (left) and RhN_4-C (right).

tion of *CO to *CHO needs to overcome a large free energy barrier, which is 1.00 and 2.01 eV, respectively, indicating the formation of other C_1 products *via* *CO, such as CH_3OH and CH_4, is unfavorable. Therefore, HCOOH is the predominant product of CO_2 reduction on CoS_4-C, and the PDS is $* + CO_2 + H^+ + e^- \rightarrow *HCOO$, with the U_L of −0.07 V. The reaction mechanism on the surface of CoN_4-C is quite different from that of CoS_4-C. It can be seen from Fig. 1b that the intermediate *HCOO is hydrogenated to form *HCOOH, and *COOH is hydrogenated to form *CO. *HCOOH is formed *via* the hydrogenation of *HCOO, and *CO is formed *via* the hydrogenation of *COOH. *HCOOH and *CO either desorb from the surface to generate $2e^-$ products HCOOH and CO due to the weak adsorption of *HCOOH and *CO, or occur subsequent hydrogenation to generate $6e^-$ product CH_3OH and $8e^-$ product CH_4. The PDS of the formation of HCOOH, CH_3OH and CH_4 is the step of $*HCOO + H^+ + e^- \rightarrow *HCOOH$, with a limiting potential of −0.30 V, and the PDS of the formation of CO is the step of $* + CO_2 + H^+ + e^- \rightarrow *COOH$ with U_L= −0.46 V. These results show that CoN_4-C can catalyze the reduction of CO_2 to multiple C_1 products, but suffers poor product selectivity. Obviously, CoS_4-C shows better activity and product selectivity than CoN_4-C. As shown in Fig. 2b, both NiS_4-C and NiN_4-C tend to generate HCOOH through the HCOO pathway, and the first hydrogenation step $* + CO_2 + H^+ + e^- \rightarrow *HCOO$ is the PDS, corresponding to the U_L of −0.42 and −0.66 V, respectively. So NiS_4-C exhibits better performance for HCOOH production than NiN_4-C. On RhS_4-C, as shown in Fig. 2c, CO_2RR to HCOOH *via* the *HCOO intermediate is more favorable than CO generation *via* *COOH. The first dehydrogenation step is the PDS for HCOOH formation, and the U_L is −0.84 V. For RhN_4-C, in addition to generating HCOOH, since *CO is facile to be hydrogenated to *CHO, which makes the subsequent PCET steps feasible, various products may be generated in the CO_2RR process, including CO, HCOOH, CH_3OH, CH_4, with the same PDS ($* + CO_2 + H^+ + e^- \rightarrow *COOH$). The limiting potentials of RhS_4-C and RhN_4-C are −0.84 and −1.08 V, respectively. IrS_4-C mainly generates HCOOH and CO *via* *COOH at the limiting potential of −0.93 V, while for IrN_4-C, four C_1 products CO, HCOOH, CH_3OH, and CH_4 will be produced at the limiting potential of −1.16 V. And the PDS of these two catalysts is the step of $* + CO_2 + H^+ + e^- \rightarrow *COOH$ (Fig. S3 in Supporting information). Thus, Rh/IrS_4-C also shows better activity and product selectivity than Rh/IrN_4-C.

Hydrogen evolution reaction (HER) is the main competing side reaction involved in electrocatalytic CO_2 reduction process, resulting in low Faradaic efficiency. The free energy diagrams of HER are given in Fig. 3a. It can be seen that Co-, Rh- and IrS_4-C suppress the HER in comparison with corresponding TMN_4-C SACs, while NiS_4-C shows better HER performance than NiN_4-C. Furthermore, in order to evaluate the selectivity preference, we compared the difference of the limiting potentials between CO_2RR and HER. As shown in Fig. 3b, the $U_L(CO_2RR)$ - U_L(HER) value of Co/NiS_4-C and NiN_4-C was positive, which means that they exhibit better selectivity to CO_2RR than to HER. In addition, although $U_L(CO_2RR)$ - U_L(HER) values of RhS_4-C and IrS_4-C are negative, they are more positive than the corresponding values of TMN_4-C catalysts (−0.08 V *vs.* −0.67 V; −0.43 V *vs.* −0.88 V), indicating that

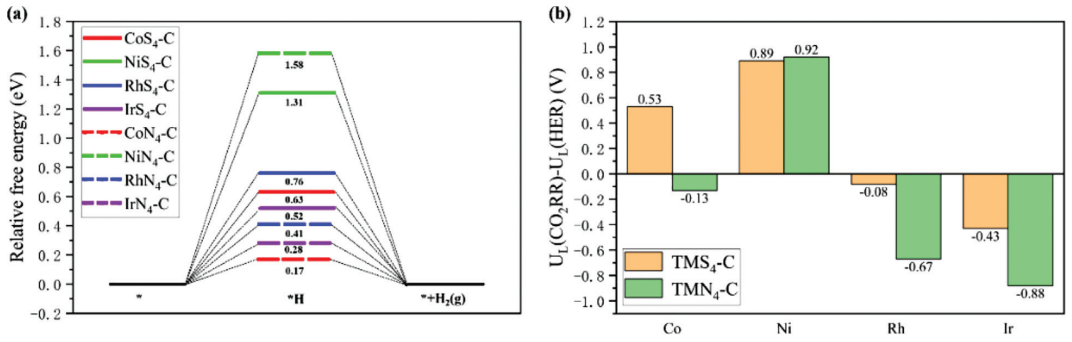

Fig. 3. (a) HER free energy profiles and (b) $U_L(CO_2RR)$ - $U_L(HER)$ of TMS_4-C and TMN_4-C catalysts.

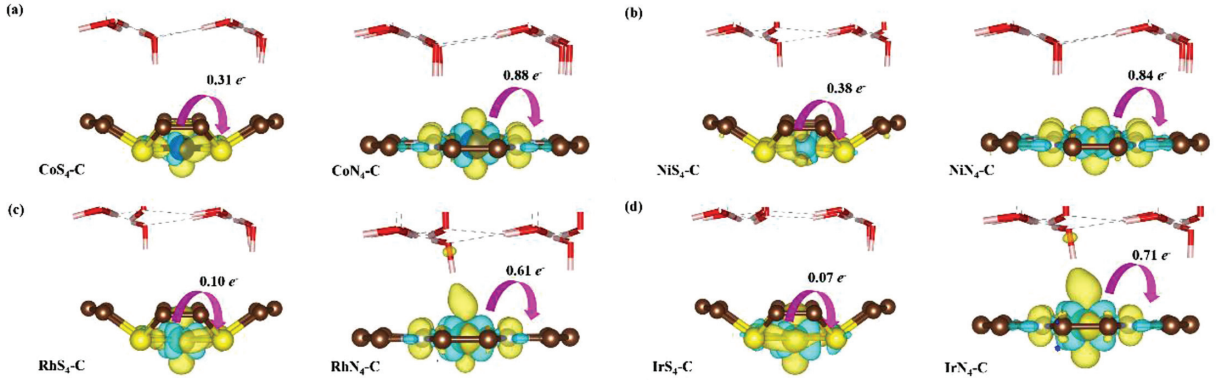

Fig. 4. Side view of CDD maps of (a) CoS_4-C and CoN_4-C, (b) NiS_4-C and NiN_4-C, (c) RhS_4-C and RhN_4-C, (d) IrS_4-C and IrN_4-C. The Co, Ni, Rh, Ir, C, N and S atoms are represented by indigo blue, light gray, tawny, olive, brown, bule and yellow balls, respectively. The H_2O molecules are represented by white-red sticks. The yellow and blue areas mean the accumulation and depletion of electron density (isosurface value: 0.01 e/Å^3). The purple arrow represents the direction of electron transfer.

compared with TMN_4-C coordination, TMS_4-C improves the selectivity of the catalyst towards CO_2RR.

The above results indicate that these TMS_4-C SANs show better activity and selectivity than widely studied TMN_4-C catalysts. Compared with Cu(211) ($U_L = -0.61$ V), CoS_4-C and NiS_4-C SANs exhibit better catalytic performance. Specially, the CoS_4-C SAN that has been prepared in experiment owns the FADH-like activity and selectivity for the production of HCOOH, and can generate HCOOH at a low U_L of -0.07 V, showing its great practical application potential. To explore the nature that TMS_4-C SANs have better catalytic activity than TMN_4-C, the electronic structure analysis of these catalysts was performed. The partial charge transfer of these two kinds of SACs was analyzed by Bader charge analysis [36]. The charge density difference (CDD) of TMS_4-C SANs and TMN_4-C SACs is plotted in Fig. 4. As can be seen from the figure, since the electronegativity of S is lower than that of N, the TM atom donates less electrons to S atoms than to N atoms, resulting in lower valence state. For the same metal, the greater the electron density of TM atom caused by the low electronegativity of S, the higher the reduction ability.

The distribution of electrons in the d_{z^2} orbitals has a great influence on the catalytic activity of SACs, because intermediates are usually axially adsorbed on the single-atom site, which has been reported in previous studies [37,38]. Here, the d-band centers of axial d_{z^2} orbitals ($\varepsilon(d_{z^2})$) of transition metals in TMS_4-C and TMN_4-C were calculated and shown in Fig. 5. It is seen that the $\varepsilon(d_{z^2})$ of TMS_4-C is closer to the Fermi level than the $\varepsilon(d_{z^2})$ of the corresponding TMN_4-C SACs, indicating that compared with TMN_4-C, the S-coordination causes the d-band centers of d_{z^2} orbitals to move upwards, thus enhancing the interaction between TMS_4-C and intermediates *HCOO (Co-, Ni-, RhS_4-C) and *COOH (IrS_4-C). As the first hydrogenation step of CO_2 to *HCOO/*COOH is the PDS of the electrocatalytic CO_2RR on TMS_4-C and TMN_4-C, the stronger interaction between TMS_4-C surface and *HCOO/*COOH makes it show better activity than TMN_4-C.

It is meaningful to explore the descriptors highly correlated to the catalytic activity in order to guide the design of novel CO_2RR electrocatalysts. Based on the intrinsic properties of the catalysts, we proposed a descriptor φ_1, which is defined as $\varphi_1 = \chi_{TM}/\chi_{NM} - N_d - N_{es}$, where χ_{TM} is the electronegativity of TM atom, χ_{NM} is the electronegativity of nonmetal atom (S or N) coordinated with the TM atom, and N_d and N_{es} are the number of d electrons and the number of electron shell layers, respectively. Fig. 6a shows that the U_L of TMS_4-C and TMN_4-C presents a linear relationship with φ_1, indicating that φ_1 can serve as an activity descriptor for CO_2RR, and the electronegativity of active center atoms and coordination atoms has a great influence on the catalytic activity. In addition, for TMS_4-C and TMN_4-C catalysts, considering the coordination environments and TM-support interaction, we plotted the variation of the limiting potentials of CO_2RR on all these SACs with

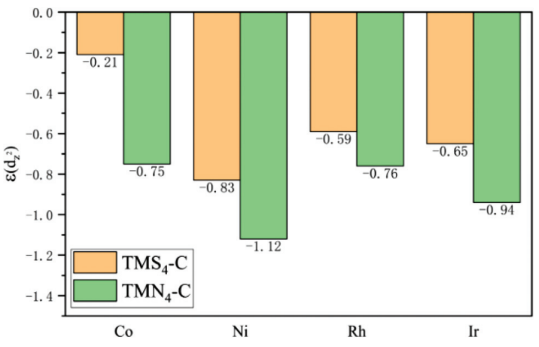

Fig. 5. $\varepsilon(d_{z^2})$ of TMS_4-C and TMN_4-C.

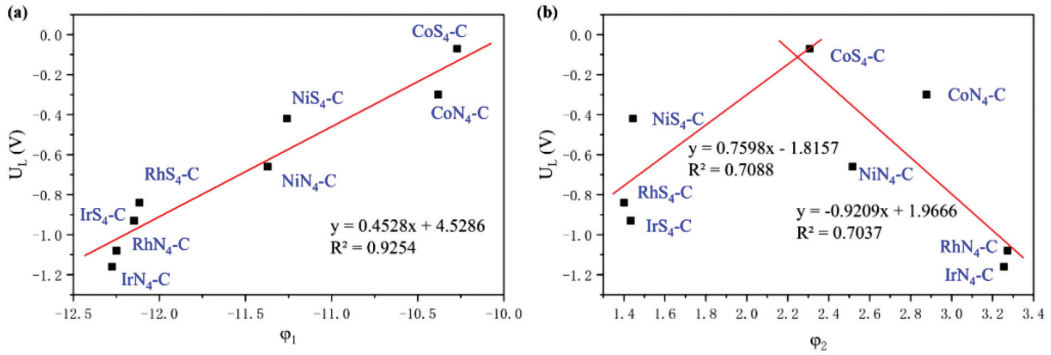

Fig. 6. (a) Linear relationship between U_L and descriptor φ_1. (b)Volcano-shape relationship between U_L and descriptor φ_2.

φ_2, where φ_2 represents the difference between the d-band center of TM atom (ε_d) and p-band center of coordinated S or N atoms (ε_p), that is, $\varphi_2 = \varepsilon_d - \varepsilon_p$. Interestingly, it can be seen from Fig. 6b that the dependence of U_L as a function of φ_2 displays a volcano-shaped curve, in which the optimal CoS_4-C SAN with the best performance for CO_2RR lies around the peak of the volcano, with φ_2 of 2.31. Thus, φ_2 can be used as a good descriptor to exhibit the CO_2RR activity. The finding of these two descriptors with reliable R^2 will be beneficial to give a reliable prediction for the catalytic ability of more similar systems.

In summary, we designed carbon-supported Group VIII TMS_4-C single-atom nanozymes (SANs) with FADH-mimic TMS_4 sites for electrochemical CO_2 reduction reaction (eCO_2RR) through DFT calculations combined with the hybrid solvation model. After the evaluation of thermodynamic and electrochemical stability, four transition metal Co, Ni, Rh and Ir SANs were selected to study the CO_2RR mechanism, and their catalytic performance was compared with that of TMN_4-C. Gibbs free energy profiles show that TMS_4-C selectively reduces CO_2 to HCOOH, while TMN_4-C generates multiple C1 products. Moreover, TMS_4-C SANs show better catalytic ability toward CO_2RR than corresponding TMN_4-C SACs, which can be attributed to the more electrons on TM atoms and the upshift of d-band center of d_{z^2} orbitals to the Fermi level. More importantly, the origin of the CO_2RR activity of TMS_4-C and TMN_4-C is revealed by the two descriptors (φ_1 and φ_2), which are highly related to the intrinsic parameters and electronic structure properties. The limiting potentials of these catalysts exhibit a volcano-shaped curve with φ_2, and CoS_4-C stands near the top of the volcano. Its U_L (−0.07 V) is far lower than the results reported previously, indicating that CoS_4-C is a potential SAN catalyst for CO_2 reduction. These findings are helpful to predict the catalytic activity of SACs and can provide new clues and ideas for the design of novel electrocatalysts for CO_2 reduction.

Declaration of competing interest

The authors declare that they have no known competing financial interests or personal relationships that could have appeared to influence the work reported in this paper.

Acknowledgments

This work was supported by the National Key Research and Development Program of China (No. 2021YFA1500403), and the National Natural Science Foundation of China (No. 21773083).

Supplementary materials

Supplementary material associated with this article can be found, in the online version, at doi:10.1016/j.cclet.2022.108018.

References

[1] D.T. Whipple, P.J.A. Kenis, J. Phys. Chem. Lett. 1 (2010) 3451–3458.
[2] J. Artz, T.E. Müller, K. Thenert, et al., Chem. Rev. 118 (2018) 434–504.
[3] H.Y. Yang, C.Z. He, L. Fu, et al., Chin. Chem. Lett. 32 (2021) 3202–3206.
[4] T.T. Cui, Y.P. Wang, T. Ye, et al., Angew. Chem. Int. Ed. 61 (2022) e202115219.
[5] L. Fu, R. Wang, C.X. Zhao, et al., Chem. Engin. J. 414 (2021) 128857.
[6] Y.C. Wang, Y. Liu, W. Liu, et al., Energy Environ. Sci. 13 (2020) 4609–4624.
[7] Y. Liu, Q.G. Feng, W. Liu, et al., Nano Energy 81 (2021) 105641.
[8] Y.C. Wang, Q.C. Wang, J. Wu, et al., Nano Energy 103 (2022) 107815.
[9] F.P. Pan, Y. Yang, Energy Environ. Sci. 13 (2020) 2275.
[10] L.M. Wang, W.L. Chen, D.D. Zhang, et al., Chem. Soc. Rev. 48 (2019) 5310.
[11] M. Sha, W.Q. Xu, Z.C. Wu, W.L. Gu, C.Z. Zhu, Chem. J. Chin. U. 43 (2022) 20220077.
[12] Y. Wang, K. Qi, S.S. Yu, et al., Nano-Micro Lett. 11 (2019) 102.
[13] L. Jiao, W.Q. Xu, Y. Zhang, et al., Nano Today 35 (2020) 100971.
[14] B.T. Qiao, A.Q. Wang, X.F. Yang, et al., Nat. Chem. 3 (2011) 634–641.
[15] X.H. Sun, L. Sun, G.N. Li, et al., Angew. Chem. Int. Ed. 61 (2022) e202207677.
[16] L.H. Shen, D.X. Ye, H.B. Zhao, J.J. Zhang, Anal. Chem. 93 (2021) 1221–1231.
[17] Z. Lin, L.L. Zheng, W.S. Yao, et al., J. Mater. Chem. B 8 (2020) 8599.
[18] H.Y. Ruan, S.F. Zhang, H.G. Wang, et al., ACS Appl. Nano Mater. 5 (2022) 6564–6574.
[19] B. Jiang, Z.J. Guo, M.M. Liang, Nano Res. 16 (2023) 1878–1889.
[20] L. Jiao, J.B. Wu, H. Zhong, et al., ACS Catal. 10 (2020) 6422–6429.
[21] L. Huang, J.X. Chen, L.F. Gan, J. Wang, S.J. Dong, Sci. Adv. 5 (2019) eaav5490.
[22] L. Wen, C.J. Ren, Y. Zou, K.N. Ding, Appl. Surf. Sci. 534 (2020) 147595.
[23] Y. Zhou, S.T. Liu, Y.M. Gu, et al., J. Am. Chem. Soc. 143 (2021) 14071–14076.
[24] N.N. Li, C. Zhu, J.W. Zhang, et al., Chem. Commun. 57 (2021) 5302 57, 5302.
[25] G. Kresse, J. Furthmüller, Phys. Rev. B 54 (1996) 11169–11186.
[26] G. G. Kresse, J. Hafner, Phys. Rev. B 47 (1993) 558–561.
[27] P.E. Blöchl, Phys. Rev. B: Condens. Matter Mater. Phys. 50 (1994) 17953.
[28] J.P. Perdew, K. Burke, M. Ernzerhof, Phys. Rev. Lett. 77 (1996) 3865.
[29] S. Grimme, J. Antony, S. Ehrlich, H. Krieg, J. Chem. Phys. 132 (2010) 154104.
[30] J. Wang, M.Y. Zheng, X. Zhao, W.L. Fan, ACS Catal. 12 (2022) 5441–5454.
[31] M. Qin, X. Meng, W. Wang, Chem. Phys. Lett. 765 (2021) 138321.
[32] X. Xie, K.L. Wang, M.H. Wei, et al., J. Electrochem. Soc. 169 (2022) 044521.
[33] K. Mathew, R. Sundararaman, K. Letchworth-Weaver, T.A. Arias, R.G. Hennig, J. Chem. Phys. 140 (2014) 084106.
[34] X.Y. Guo, S.R. Lin, J.X. Gu, et al., ACS Catal. 9 (2019) 11042–11054.
[35] A.A. Peterson, F. Abild-Pedersen, F. Studt, J. Rossmeisl, J.K. Nørskov, Energy Environ. Sci. 3 (2010) 1311–1315.
[36] G. Henkelman, A. Arnaldsson, H. Jónsson, Comput. Mater. Sci. 36 (2006) 354–360.
[37] W.Q. Xu, Y.K. Kang, L. Jiao, et al., Nano-Micro Lett. 12 (2020) 184.
[38] Y.J. Ji, H.L. Dong, C. Liu, Y.Y. Li, Nanoscale 11 (2019) 454.